Static and Dynamic Light Scattering from Polystyrene/Poly(methyl methacrylate)/Bromobenzene: Temperature Effects

J. Seils,* M. Benmouna, A. Patkowski,† and E. W. Fischer

Max-Planck-Institut für Polymerforschung, Ackermannweg 10, 55128 Mainz, Germany

*Received March 7, 1994; Revised Manuscript Received June 3, 1994**

ABSTRACT: Static and dynamic light scattering measurements on polystyrene/poly(methyl methacrylate)/bromobenzene solutions under the optical Θ condition are reported. The Θ condition is fulfilled by knowing that the average increment of refractive index of the two polymers is zero and letting their composition be 1/2. The total polymer concentration is kept constant and the temperature is changed from 30 °C to the critical temperature T_c which is found at 2 °C. The results reveal two distinct ranges of temperatures where both static and dynamic properties show different behaviors. The upper range of temperatures which is above 7 °C in this mixture can be described quite well with the mean field model based on the random phase approximation. In particular the dynamic scattering function relaxes with a single exponential whose decay rate fits well to the theoretical prediction using the above approximation. Below 7 °C, the results show strong effects of the critical fluctuations which manifest themselves in the static properties by critical exponents of the Ising type. The dynamic correlation function decays by following a bimodal distribution and the slow mode decays according to the critical slowing down, as predicted by the mode coupling theory. The first cumulant of the dynamic scattering function is analyzed as a function of the temperature, and good agreement is found with the theoretical framework based on the mode coupling model and using the measured structure factor. From the intermediate q region where the first cumulant has a q^3 behavior, the viscosity of the mixture is deduced and analyzed as a function of temperature.

1. Introduction

Recently, substantial progress has been made in understanding the dynamics of ternary mixtures made of two polymers and a solvent.[1-4] Using the random phase approximation (RPA), one can express concentration and composition fluctuations in these mixtures in terms of single chain structure factors, diffusion coefficients, and Flory-Huggins interaction parameters. Under certain conditions the measurable dynamic and static structure factors simplify considerably and depend directly on the composition fluctuations. It was shown that the ternary mixture under such conditions can be treated as a quasi-binary mixture of two polymers swollen by a common solvent. Analogous to binary mixtures, the interdiffusion process shows a critical slowing down and the static structure factor tends to diverge when the system approaches its critical temperature of phase separation. In view of the observed crossover from mean-field to Ising exponents in binary polymer blends,[5-7] it is expected[3] that a similar crossover could be observed in ternary mixtures in the presence of a low molecular weight solvent with a broader transition region.

Far from the critical conditions[8-11] it was shown by dynamic light scattering that two relaxation modes describe the dynamics of these mixtures. One is the usual cooperative mode which is due to the fluctuations in the total polymer concentration and relaxes faster as the average concentration increases. This process is not very sensitive to the chemical mismatch of the two polymer species, and therefore it is not relevant in the present study. The other mode reflects the polymer composition fluctuations which are much more sensitive to the chemical mismatch of the polymer species, and their relaxation slows down critically when approaching the critical temperature.

Since the properties of these systems are known as a function of mean concentration and composition at room temperature,[8-11] and considering the importance of both static and dynamic properties of polymer mixtures in the vicinity of the critical conditions, we undertake here a light scattering study of the temperature effects by keeping the mean concentration and composition constant. We examine the case of a symmetric blend satisfying the so-called optical Θ condition. In this case, the mean-field theory predicts that only one relaxation mode is observed and can be interpreted as the interdiffusion due to the polymer composition fluctuations. Combining total intensity and dynamic light scattering measurements, we examine the behavior of static and dynamic properties independently which allows us to check the approximations made in the theory and pinpoint its limitations.

In section 2 we review the basic equations describing the static and dynamic scattering properties of ternary mixtures using the RPA. This allows us to give the explicit form of the cross correlation of composition and concentration fluctuations within the latter approximation. An ad hoc assumption is made to extend these results to the vicinity of the critical temperature for spinodal decomposition. This assumption enables us to define a transition from the mean-field region where the RPA is useful to the critical region where Ising-like exponents are observed. In section 3 the experimental conditions and relation between the theoretical quantities and the measured ones are discussed. In section 4, the results and their interpretations are presented. The last section gives further discussions of the results and the conclusions.

2. Theory

2.1. Integrated Intensity. For a mixture of polymer species A and B in a solvent the total scattered light intensity as a function of scattering wavevector q is given using RPA[12] and the incompressibility assumption by

$$I(q) = \alpha^{\mathrm{T}} \begin{pmatrix} \dfrac{S_A^0(1+\delta_{BS}S_B^0)}{D} & -\dfrac{\delta_{AB}S_A^0S_B^0}{D} \\ -\dfrac{\delta_{BA}S_A^0S_B^0}{D} & \dfrac{S_B^0(1+\delta_{AS}S_A^0)}{D} \end{pmatrix} \alpha \quad (1a)$$

† Also at the Institute of Physics, A. Mickiewicz University, Poznan, Poland.

* Abstract published in *Advance ACS Abstracts*, July 15, 1994.

0024-9297/94/2227-5043$04.50/0

The denominator D is obtained as

$$D = 1 + \delta_{AS}S_A^0 + \delta_{BS}S_A^0 - \delta_{AB}\delta_{BA}S_A^0S_B^0 + \delta_{AS}\delta_{BS}S_A^0S_B^0 \quad (1b)$$

q is related to the wavelength of the incident light λ, the scattering angle θ, and the index of refraction of the medium n_r by

$$q = \frac{4\pi}{\lambda}n_r \sin\left(\frac{\theta}{2}\right) \quad (2)$$

In eq 1a, α is the column vector of the mean molecular polarizabilities α_M^A and α_M^B, α^T is its transpose, δ_{BS}, δ_{AS}, and δ_{AB} are the excluded volumes, and χ_{AB} is the interaction parameter between polymers A and B:

$$\chi_{AB} = \delta_{AB} - \frac{\delta_{AS}}{2} - \frac{\delta_{BS}}{2} \quad (3)$$

In the starting RPA eqs 1a and 1b, the bare structure factors are defined by

$$S_A^0 = x\Phi n_A P_A(q) \quad (4)$$

where $x = \Phi_A/(\Phi_A + \Phi_B)$ is the mean composition of A, $\Phi = \Phi_A + \Phi_B$ is the total volume fraction of the polymer, n_A is the degree of polymerization, and P_A is the single chain form factor of A. Equations 1–4 express the scattered light intensity in terms of the partial structure factors S_{ij} using the RPA. Rewriting (1a), one has

$$I(q) = \alpha^T\begin{pmatrix} S_{AA} & S_{AB} \\ S_{BA} & S_{BB}\end{pmatrix}\alpha = \alpha^T\tilde{S}(q)\alpha \quad (5)$$

In the particular conditions of our system, the scattered intensity can be expressed in terms of $S_{cc}(q)$ and $S_{xx}(q)$ which represent the structure factors for concentration and composition fluctuations, respectively. These quantities are combinations of $S_{ij}(q)$ and can be determined by operating on $\tilde{S}(q)$ by the following transformation:

$$S(q) = \begin{pmatrix} S_{cc} & S_{cx} \\ S_{xc} & S_{xx}\end{pmatrix} = \mathbf{a}^T\begin{pmatrix} S_{AA} & S_{AB} \\ S_{BA} & S_{BB}\end{pmatrix}\mathbf{a} \quad (6a)$$

where $\mathbf{a}$ is defined by

$$\mathbf{a}^T = \begin{pmatrix} 1 & 1 \\ 1-x & -x\end{pmatrix} \quad (6b)$$

Combining eqs 5 and 6 yields the scattering intensity $I(q)$ as

$$I(q) = [\alpha_M^A x + \alpha_M^B(1-x)]^2S_{cc}(q) + [\alpha_M^A - \alpha_M^B]^2S_{xx}(q) + 2[\alpha_M^A x + \alpha_M^B(1-x)][\alpha_M^A - \alpha_M^B]S_{xc}(q) \quad (7a)$$

It is clear that if one works in the so-called optical Θ conditions defined by

$$\alpha_M^A x + \alpha_M^B(1-x) = 0 \quad (7b)$$

one finds that the scattered intensity is directly proportional to $S_{xx}(q)$:

$$I(q) = (\alpha_M^A - \alpha_M^B)^2S_{xx}(q) \quad (7c)$$

One can determine $S_{xx}(q)$ in terms of the known structure factors $S_{ij}(q)$ from eq 6 and obtain

$$S(q) = \begin{pmatrix} S_{AA} + 2S_{AB} + S_{BB} & (1-x)(S_{AA} + S_{AB}) - x(S_{BB} + S_{AB}) \\ (1-x)(S_{AA} + S_{AB}) - x(S_{BB} + S_{AB}) & (1-x)^2S_{AA} + x^2S_{BB} - 2x(1-x)S_{AB}\end{pmatrix} \quad (8a)$$

This result is interesting not only because it gives the definitions of S_{xx} and S_{cc} in terms of $S_{ij}(q)$ but also because it gives the coupling term S_{xc}:

$$S_{cx} = S_{xc} = (1-x)(S_{AA} + S_{AB}) - x(S_{BB} + S_{BA}) \quad (8b)$$

According to ref 4, this result seems to be new since the cross correlation S_{xc} has not been reported explicitly before. In the conditions of a symmetric mixture where the polymers have approximately the same size and the same interaction with the solvent but they are characterized by a finite interaction between different species ($\chi_{AB} \neq 0$), one has $S_{AA} = S_{BB}$. This equality is completely achieved only if the composition x is 1/2. In this case, the coupling between concentration and composition fluctuations vanishes and the pair S_{xx} and S_{cc} coincide with the eigenvalues of $\tilde{S}(q)$. Equation 6a becomes

$$S(q) = \begin{pmatrix} S_{AA} + S_{BB} + 2S_{AB} & 0 \\ 0 & \frac{1}{4}(S_{AA} + S_{BB} - 2S_{AB})\end{pmatrix} \quad (8c)$$

from which we deduce

$$S_{xx}(q) = \frac{1}{4}(S_{AA} + S_{BB} - 2S_{AB}) \quad (9)$$

2.2. Dynamics. A similar procedure can be used to describe the dynamical scattering functions. The equation of motion for the diagonal dynamic structure matrix $\mathbf{S}(q,t)$ can be obtained by different methods[12–14] and in particular by using the Mori–Zwanzig projection operator formalism.[15] Ignoring memory effects, one gets the simple equation

$$\frac{\partial}{\partial t}\mathbf{S}(q,t) = -\bar{\Gamma}(q)\mathbf{S}(q,t) \quad (10)$$

For a symmetrical mixture all the matrices in this equation are diagonal. The first cumulant $\bar{\Gamma}(q)$ is related to the generalized Onsager mobility $M(q)$ according to

$$\bar{\Gamma}(q) = \frac{q^2kT\mathbf{M}(q)}{\mathbf{S}(q)} \quad (11)$$

k is the Boltzmann constant and T the absolute temperature. Using the Oseen tensor description for the hydrodynamic interaction[13,14] and assuming that the friction coefficients of both polymers are equal to $\zeta = 3\pi\eta a$, where η is the viscosity of the medium and a the statistical length, one obtains

$$\mathbf{M}(q) = \frac{1}{\eta} \times \begin{pmatrix} \frac{\Phi}{3\pi a} + \frac{1}{4\pi^2}\int_0^\infty dq' f\left(\frac{q'}{q}\right)S_{cc}(q') & 0 \\ 0 & \frac{\Phi}{3\pi a} + \frac{1}{4\pi^2}\int_0^\infty dq' f\left(\frac{q'}{q}\right)S_{xx}(q')\end{pmatrix} \quad (12)$$

where $f(x)$ is given by

$$f(x) = x^2\left(\frac{x^2+1}{2x}\ln\left|\frac{x+1}{x-1}\right| - 1\right) \quad (13)$$

2.3. Critical Behavior. Since we are essentially interested in the long range fluctuations taking place near the critical temperature, it is sufficient to approximate the single chain form factor $P(q)$ by the leading contribu-

tion

$$P(q) = \frac{1}{1 + \frac{1}{3}q^2R_g^2} \tag{14}$$

In this case the static structure factor $S_{xx}(q)$ has the Ornstein–Zernike form:

$$S_{xx}^{-1} = 2(\chi_{mc} - \chi_{AB}) + \frac{4R_g^2}{3n\Phi}q^2 \tag{15a}$$

with

$$\chi_{mc} = \frac{2}{n\Phi} \tag{15b}$$

R_g is the radius of gyration and n the degree of polymerization. Equation 15a can be written in terms of the structure factor $S_{xx}(q=0)$ and the correlation length ξ_m; the subscript m represents the mean-field limit and should be distinguished from the critical limit obtained near T_c. One writes

$$S_{xx}(q)^{-1} = S_{xx}(q=0)^{-1}(1 + q^2\xi_m^2) \tag{16a}$$

with

$$S_{xx}(q=0)^{-1} = 2(\chi_{mc} - \chi_{AB}) \tag{16b}$$

$$\xi_m^2 = \frac{2R_g^2}{3n\varphi(\chi_{mc} - \chi_{AB})} \tag{16c}$$

It is assumed further that the temperature dependence of the interaction parameter χ_{AB} can be described by

$$\chi_{AB}(T) = \frac{\chi_{AB}^A}{T} + \chi_{AB}^B \tag{17}$$

where the constants χ_{AB}^A and χ_{AB}^B are independent of the temperature and depend only on the nature of the polymers. Combining eqs 16 and 17 yields the correlation length in the mean-field approximation

$$\xi_m = R_g\left(\frac{T_{mc}\chi_{mc}}{3\chi_{AB}^A}\right)^{1/2}\epsilon_m^{-\nu_m} \qquad \nu_m = 0.5 \tag{18a}$$

and the inverse structure factor in the forward direction

$$S_{xx}^{-1} = \frac{2\chi_{AB}^A}{T_{mc}}\epsilon_m^{\gamma_m} \qquad \gamma_m = 1 \tag{18b}$$

where ϵ_m is defined by

$$\epsilon_m = \frac{T - T_{mc}}{T} \tag{18c}$$

In writing these equations we have deliberately introduced the scaling laws of the correlation length and the scattering intensity in the forward direction by anticipating the discussions of their scaling behavior in the vicinity of T_c. It is important to keep in mind that the above results are obtained within the mean-field approximation and, as such, they are meant to describe only the properties far from the experimental critical temperature. In the above equations, we have introduced the quantities χ_{mc} and T_{mc} which represent the critical interaction parameter and critical temperature in the mean-field description (see eq 15b). A clear distinction is made between the latter quantity and the real T_c observed experimentally. If T_c is approached, the above results should be modified in a way to account for the effects of critical fluctuations. This is done here using the ad hoc assumption that the form of these equations remains valid but the critical exponents should be modified in such a way that ν_m and γ_m are replaced by the Ising exponents:

$$\nu = 0.63 \tag{19a}$$

$$\gamma = 1.24 \tag{19b}$$

Table 1. Polymers and Solvent Characteristics

	PS	PMMA	bromobenzene
M_w	9.1×10^5	9.8×10^5	
M_w/M_n	1.15	1.07	
N_W	8750	9800	
M_M	104	100	
$dn_r/d\Phi$	0.0518	−0.0607	
ρ (g/cm^3)	1.070	1.212	1.495
c (g/L)	22	22	
Φ	0.020	0.018	
n_r			1.56
	Other and Average Quantities		
λ (nm)	488		
$\bar{\rho}$ (g/cm^3)	1.136		
$(dn_r/d\Phi)^2$	0.003 15		
$\bar{M}_M$	102.125		
ΦN	355		

3. Experimental Section

3.1. Samples. Polystyrene was synthesized by anionic polymerization by a procedure described elsewhere.[16] Poly(methyl methacrylate) was purchased from Polymer Standards Services (Mainz, Germany). The molecular weight distributions of both polymers were characterized by gel permeation chromatography. The relevant parameters characterizing the polymers and the solvent are summarized in Table 1. Two stock solutions were prepared by dissolving 45 mg/mL of each of the polymers in bromobenzene which was vacuum-distilled into a flask containing dried molecular sieves directly before sample preparation. The stock solutions were gently shaken for 24 h. After the polymers were completely dissolved, molecular sieves were added to the solutions. Then 5 mL of the PS solution was added to 5 mL of the PMMA solution. Since the resulting solution was phase separated, a controlled amount of bromobenzene was added to enter the one phase region at room temperature. The final total polymer concentration was 44 mg/mL. Dried molecular sieves were also added to the mixture.

For the light scattering experiments, the sample solutions were filtered through a Millipore filter with an average pore size of 0.45 μm directly into a dust-free light scattering cell with $^1/_2$-in. outer diameter. The sample cell was then connected to a high vacuum line, frozen by putting it into a thermostated can with liquid nitrogen, and evacuated. The high vacuum line was equipped with a porous filter on the sample entrance in order to avoid dust particles. After evacuation, the sample was allowed to warm up. By several cooling and warming cycles the sample was degassed and finally flame-sealed.

3.2. Light Scattering. Total intensity light scattering measurements were performed at temperatures ranging from 30 to 2 °C in a scattering angle range from θ = 10 to 130° in steps of 1° using the ALV goniometer with a ceramic cell. The sample cell was sitting in a toluene bath to index match the cell surface and outer medium. By this and the relative high scattered light intensities it was possible to measure down to such low angles covering a q range from 3.46×10^4 to 3.60×10^5 cm^{-1}. The cell was heated by a thermostat with external temperature control better than ±0.02 K. As a light source an argon ion laser (Spectra Physics Model 165) operating at 488 nm with an output power of 100 mW was used. The laser beam was split with a 50/50 beam splitter to use it on two setups at the same time. Incident and scattered beams were polarized perpendicular to the scattering plane (VV geometry). In front of the polarizer for the incident beam a second polarizer was mounted which could be rotated off VV in order to attenuate the power of the beam entering the scattering cell. The beam was attenuated to get a maximum of 3×10^5 photons/s at the lowest scattering angle detected with a photomultiplier (EMI 9863) operating in the single photon counting mode.

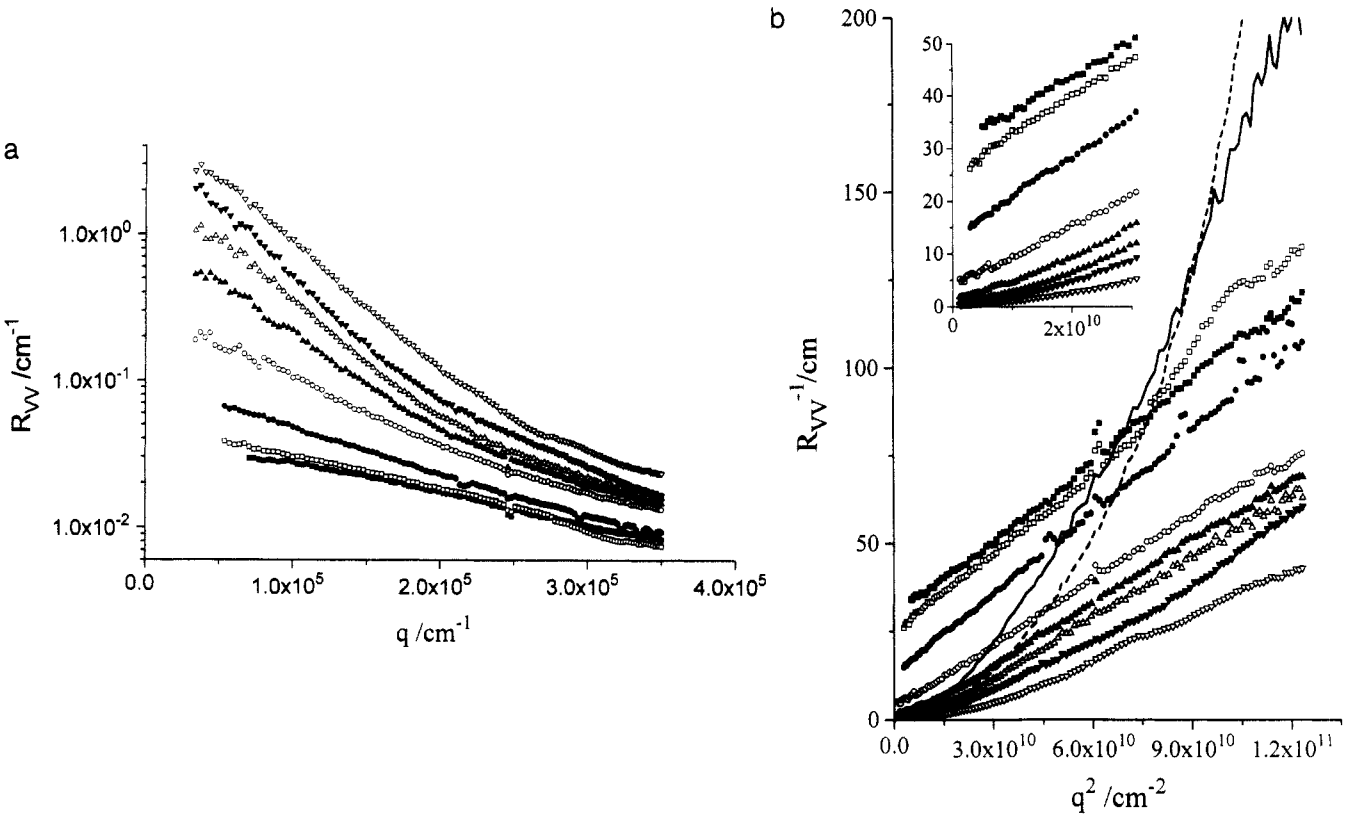

Figure 1. (a) Absolute Rayleigh ratios $R_{VV}(q)$ as a function of the amplitude of the wave vector q for different temperatures. The temperatures from top to bottom are (▽) 2.5 °C, (▼) 3 °C, (△) 4 °C, (▲) 5 °C, (○) 7 °C, (●) 10 °C, (□) 20 °C, and (■) 30 °C. (b) Ornstein–Zernike plots for PS/PMMA/bromobenzene for different temperatures. The symbols corresponding to different T's are the same as in Figure 1a. The solid and dashed lines represent the scattered light intensities calculated from the relative amplitudes of the slow mode detected at T = 277 K and T = 276 K by inverse Laplace transform of the intensity autocorrelation functions. The insert shows an extended view of the low q region to indicate the curvature in the Ornstein–Zernike plots at low q.

Autocorrelation functions were measured with an ALV 5000 correlator in a scattering angle range from θ = 10 to 120°. The measured angles were chosen in such a way that an almost linear q spacing was achieved. Other conditions were the same as for the total intensity measurements. The incident beam was attenuated at each scattering angle to get an average scattered intensity of 1 × 10^5 photons/s. Each correlation function was then accumulated for 40 min. By this procedure similar statistical noise and exactly the same time ranges were covered for all measurements.

3.3. Measurable Quantities. The scattered light intensities measured are proportional to the static structure factors. The proportionality constants depend on a number of parameters which are specific to the setup used here. Absolute intensities can be obtained by using a known reference sample and calculating the excess Rayleigh ratio R_{VV} for the composition fluctuations.

$$R_{VV} = \frac{I_T(q) - I_B(q)}{I_{ref}} \left(\frac{n_r}{n_r^{ref}}\right)^2 R_{VV}^{ref} \tag{20}$$

Here $I_B(q)$ is the average weighted scattered intensity of the two binary polymer solvent systems with the same total polymer concentration as the ternary mixture which has scattered light intensity $I_T(q)$ under the same conditions. The weighting factors in general depend on the refractive index increments of the two polymers. Since the intensities for the binary polymer solutions are at least a factor of 1000 lower than $I_T(q)$ and the weights are much smaller than 1 when the optical Θ condition is almost fulfilled, we set $I_B(q)$ to zero. I_{ref} is the scattered intensity of the reference sample under the same conditions. The factor containing the refractive indices n, and n_r^{ref} is a scattering volume correction due to the different focusing of the laser beam on the sample and the reference, respectively. Finally, R_{VV}^{ref} is the known Rayleigh ratio of the reference sample. For toluene it is given by Bender et al.[17] as 3.01 × 10^{-5} cm^{-1} at the wavelength λ = 488 nm. With these parameters one can calculate the static structure factor due to composition fluctuations via

$$S_{xx}(q) = \frac{R_{VV}(q)\lambda^4 \bar{\rho} \mathcal{N}_A}{4\pi^2 n_r^2 (dn_r/d\Phi)^2 \bar{M}_M} \tag{21}$$

Here $\bar{\rho}$ and $\bar{M}_M$ are defined by

$$\bar{\rho} = (\Phi_A \rho_A + \Phi_B \rho_B)/\Phi \tag{22}$$

$$\bar{M}_M = (\Phi_A M_M^A + \Phi_B M_M^B)/\Phi \tag{23}$$

They correspond to the mean density and molecular weight of monomers A and B, respectively; $\mathcal{N}_A$ is the Avogadro number. In deriving eq 21, it is assumed that the molecular volumes of solvent and both monomers are the same.

With photon correlation spectroscopy in the homodyne detection method the second-order or intensity autocorrelation function is measured, which directly gives the square of the normalized dynamic structure factor. In the most general case the square root of this quantity gives a distribution $G(\Gamma)$ of relaxational processes

$$\left(\left(\frac{S(q,t)}{S(q,0)}\right)^2\right)^{1/2} = \int_0^\infty G(\Gamma) \exp(-\Gamma t)\, d\Gamma \tag{24}$$

from which one obtains the first cumulant by

$$\bar{\Gamma} = \frac{\int_0^\infty \Gamma G(\Gamma)\, d\Gamma}{\int_0^\infty G(\Gamma)\, d\Gamma} \tag{25}$$

3.4. Data Corrections. Typical scattered light intensities for critical mixtures are rather high. Therefore the intensities have to be corrected for turbidity and eventually also for multiple

Table 2. Experimentally Determined Quantities (T_c = 275.4 K)

ϵ	R_0 (cm^{-1})	ξ (nm)	$D_I(0)$ (cm^2/s)	η (cP)
0.0915	0.033	39.7	1.96×10^{-9}	23.69
0.0606	0.039	61.1	1.66×10^{-9}	27.57
0.0274	0.075	99.5	9.52×10^{-10}	33.88
0.0170	0.230	128.4	9.47×10^{-10}	36.84
0.0099	0.667	167.0	5.29×10^{-10}	44.78
0.0063	1.276	230.0	3.40×10^{-10}	52.80
0.0027	2.993	324.0	2.88×10^{-10}	51.13

remark	χ_C	χ^A_{AB} (K)	χ^B_{AB}
from eqs 17, 18	$(1.1 \pm 0.1) \times 10^{-3}$	1.8 ± 0.2	$(-5.3 \pm 0.8) \times 10^{-3}$
from eq 15b	5.6×10^{-3}		

scattering. The turbidity correction is given by

$$I_C(q) = I_M(q)\frac{T_{ref}}{T_s} \tag{26}$$

where $I_C(q)$ is the corrected scattered intensity, $I_M(q)$ is the measured scattered intensity, and T_{ref} and T_s are the measured transmissions of the reference and sample, respectively.

Multiple scattering corrections are notoriously difficult. The contribution of double scattered light can be included by the theory of Shanks and Sengers.[18] The lowest transmission we obtained for our sample at T = 276.15 K was 64%. For such transmissions double scattering corrections are very small, so they were not applied.

4. Results

4.1. Static Light Scattering. Rayleigh ratios as a function of the scattering vector q for different temperatures are shown in Figure 1a. These plots illustrate the dramatic increase of the forward intensity (a factor of 400) when the temperature is lowered from 30 to 2.5°. In order to see if these curves follow the usual Ornstein–Zernike (OZ) behavior, the same data are plotted in the appropriate coordinate system (i.e. $R_{VV}^{-1}(q)$ vs q^2) in Figure 1b. One observes that in the temperature range above 7 °C, the curves show a linear variation without distortion in the whole q range. However, for temperatures below 7 °C, a marked curvature shows up in the lower q range, indicating that the sample undergoes a different kind of fluctuation. The insert in this figure illustrates in more detail the inverse scattered intensity in the low q range. It is this range which is used to derive both the correlation length and the intercept of the scattered intensity with the axis q = 0 ($R_0 \equiv R_{VV}(q=0)$ represents the scattering in the forward direction). The results are listed in Table 2. They are illustrated further in the following figures. Figure 2a shows the variation of $R_{VV}^{-1}(q=0)$ as a function of $1/T$ with and without the correction for a static background represented by the triangles and the squares, respectively. The noncorrected data show a crossover below 7 °C, but no characteristic mean-field behavior can be seen at high temperatures. This is due to the fact that the intensity contains a constant contribution which does not exhibit a critical behavior as it is demonstrated in our quasi-elastic light scattering measurements (see Figures 4 and 5). The value of the background is obtained from the dynamic data measured at low temperatures (where it can be clearly resolved) and amounts to 2.44×10^{-2} cm^{-1}. After subtraction of the background one observes a characteristic mean-field behavior in the upper temperature range (T > 280 K) where $R_{VV}^{-1}(q=0)$ varies linearly with $1/T$. The extrapolation of this line to the horizontal axis yields the mean-field critical temperature T_{mc} = 279 K. However, in the vicinity of this temperature, there is a deviation from the linear trend and one observes a different behavior

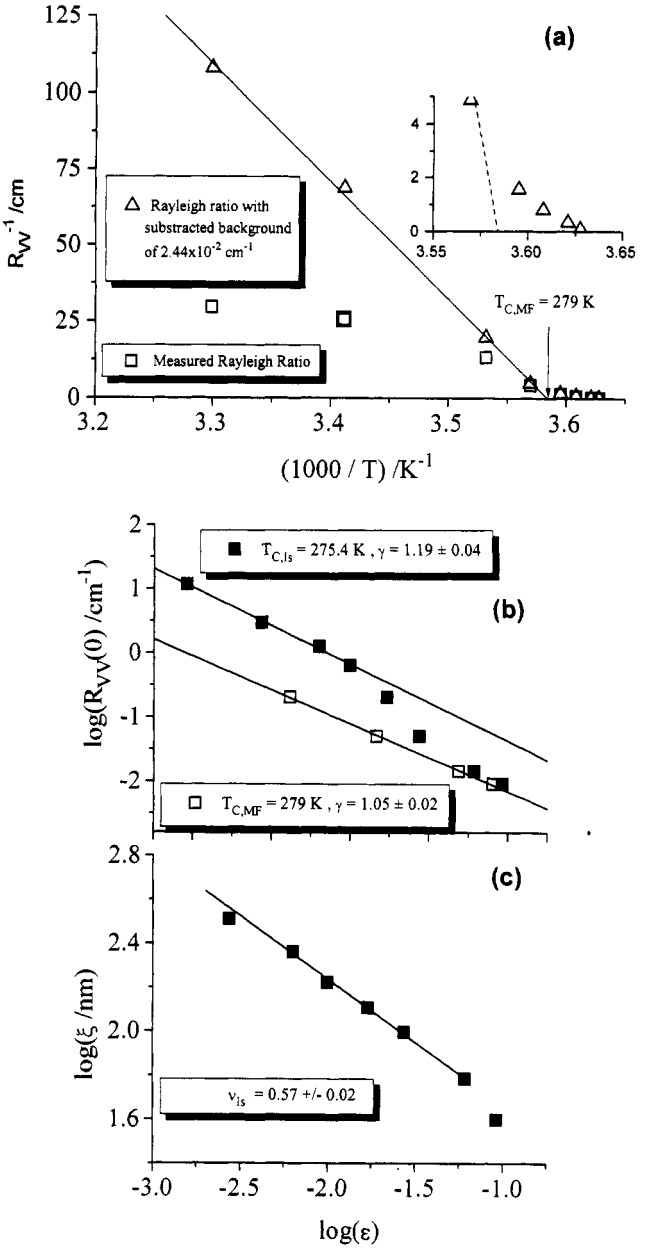

Figure 2. (a) The variation of $R_{VV}^{-1}(q=0)$ as a function of $1/T$ with the static background correction (△) and without this correction (□). The insert shows a detailed view of the crossover region from the mean-field to the Ising behavior. (b) The log of $R_{VV}(q=0)$ as a function of log ϵ. This plot enables us to calculate the exponent γ and the parameter χ^A_{AB} (see eq 19b). The open squares represent the same intensities as a function of log ϵ when ϵ is calculated using the mean field critical temperature $T_{C,MF}$. (c) The log of the correlation length ξ as a function of log ϵ. This figure allows us to determine the exponent ν and the critical parameter χ_C as seen from eq 19a and explained in the text.

leading to a lower value of the real critical temperature T_c = 275.4 K where $R_{VV}^{-1}(q=0)$ = 0. A similar observation is made in the absence of solvent for pure polymer blends.[6] In order to identify the scaling behavior of the forward scattering intensity with $(T - T_C)/T = \epsilon$, we show in Figure 2b the plot of log($R_{VV}(q=0)$) versus ϵ. If one uses the background correction of the scattering data together with the real critical temperature, one observes a crossover from the mean-field limit where γ is 1 to an Ising-like limit where γ = 1.19 (eq 19b). Other information can be obtained from this figure by considering the intercept of the curve with the vertical axis. This gives the constant χ^A_{AB} entering in the variation of χ_{AB} with T. Taking the

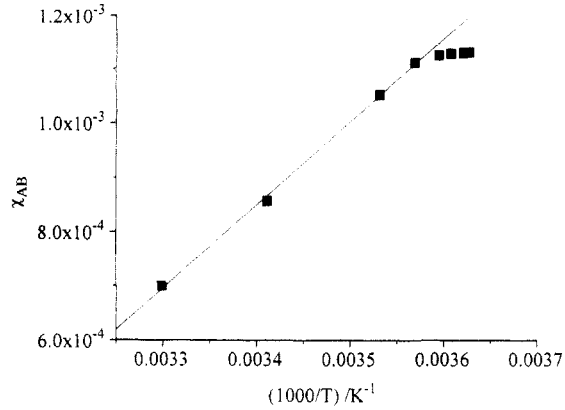

Figure 3. Variation of the Flory–Huggins interaction parameter χ_{AB} as a function of $1/T$. The solid line represents eq 18 where the constant quantities χ^B_{AB} and χ^A_{AB} are determined as explained in the text and given in Table 2.

log of eq 18b one obtains

$$\log S_{xx}^{-1} = \gamma_m \log \epsilon_m + \log\left(\frac{2\chi^A_{AB}}{T_{mc}}\right) \qquad (27a)$$

The result is $\chi^A_{AB} = 1.8 \pm 0.1$. Proceeding similarly as for the forward scattering intensity and taking the log of eq 18a one obtains

$$\log \xi = -\nu \log \epsilon + \log R_g\left(\frac{T_c\chi_c}{3\chi^A_{AB}}\right)^{1/2} \qquad (27b)$$

The plot of log ξ as a function of log ϵ is shown in Figure 2c. The correlation lengths were corrected for the background which was assumed to have an Ornstein–Zernike form with a correlation length of 47 nm obtained at the highest temperature. Using the Ising critical temperature in ϵ one finds that the exponent governing the scaling of the correlation length is $\nu = 0.57$, which is slightly lower than the expected Ising exponent 0.63 (see eq 19b). Furthermore in order to determine the complete variation of χ_{AB} with temperature one needs the quantity χ^B_{AB} which is obtained from eq 17 knowing χ_c. The latter parameter can be deduced from the intercept of the line in Figure 2c considering the high temperature range. Letting the radius of gyration to be $R_g = 47$ nm and taking the value of χ^A_{AB} derived earlier, one obtains $\chi_C = (1.11 \pm 0.1) \times 10^{-3}$, which leads to $\chi^B_{AB} = (-5.3 \pm 0.3) \times 10^{-3}$. The mean-field result given by eq 15b overestimates this quantity since $\chi_{mc} = 5.6 \times 10^{-3}$. The variation of $\chi_{AB}(T)$ as a function of $1/T$ is shown in Figure 3 and is consistent with the linear variation predicted by eq 17.

4.2. Dynamic Light Scattering. The correlation functions also show different behaviors depending on whether the temperature of the sample is below or above 7 °C. Whereas above this temperature they can be essentially described by a single exponential decay (Figure 4a), the fit fails for lower temperatures (Figure 4b). Here a double exponential fit is necessary to describe correctly the functions (Figure 4c). We performed the inverse Laplace transform with CONTIN written by S. Provencher.[19] A typical fit is displayed in Figure 4d. With the frequency distribution obtained with CONTIN one can clearly demonstrate the emergence of a second slow mode

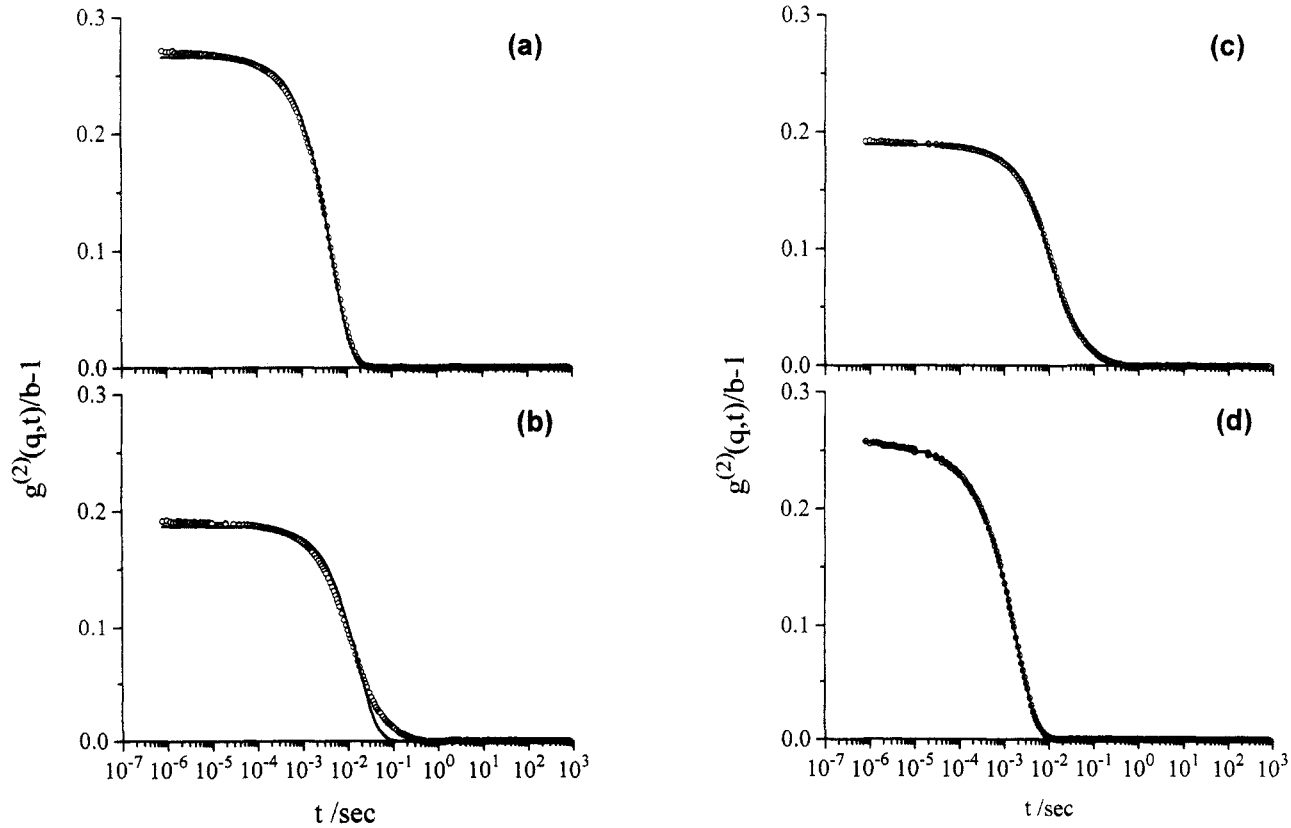

Figure 4. (a) Typical normalized intensity autocorrelation functions with fitting functions. This figure shows a single exponential fit (solid line) to the measured correlation function (open circles) at $T = 303$ K and a scattering angle $\theta = 60°$. There are small deviations from single exponential decay at short times which are caused by the presence of fast modes which contribute less than 3% to the correlation function (see Figure 5). (b) Same as Figure 4a but at $T = 278$ K. Note the strong deviations of the fitted function from the measured one at long times. (c) Same correlation function as in Figure 4b fitted to a double exponential. There are slight deviations at short times. (d) Fit to a correlation function measured at $T = 303$ K and $\theta = 90°$ when the function is described by a distribution $G(\Gamma)$ of relaxation frequencies Γ (CONTIN). The function is represented well over the whole time range. The same is true for lower temperatures.

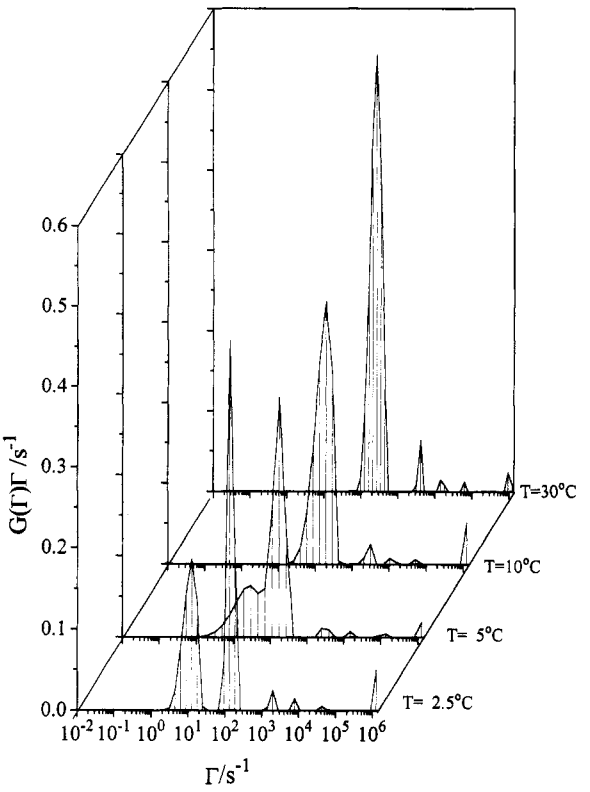

Figure 5. Frequency distributions $G(\Gamma)$ for different temperatures as obtained from CONTIN. The corresponding correlation functions were measured at $\theta = 90°$. The frequency distribution is multiplied by Γ. $\Gamma G(\Gamma)$ actually corresponds to a $\log(\tau)$ distribution.

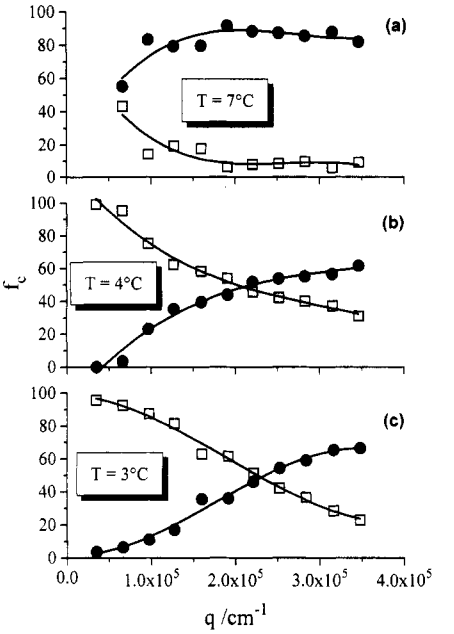

Figure 6. Relative amplitudes of the two modes as a function of scattering angle. (a) ● represents the contribution of the fast mode f_c to the intensity autocorrelation function at a temperature of 7 °C. At higher temperatures it is the only mode present where it represents the relaxation of the composition fluctuations. □ represents the slow mode which can only be detected at temperatures lower than or equal to 7 °C. The curves are polynomial fits of order 3 just as guides for the eye. (b) Same quantities as in (a) but at 4 °C. Note the switch of the two curves where at low q the slow mode contributes more to the relaxation of the composition fluctuations. (c) Dominance of the slow mode at low q further increased at 3 °C.

when the temperature is lowered (Figure 5).

As has been demonstrated earlier, the mode observed in the high temperature range is clearly due to composition fluctuations. From Figure 5 we would conclude that the composition fluctuations split into a bimodal distribution of relaxation frequencies. The question arises whether these modes show a critical slowing down. The fast mode can be observed over the whole temperature range and its relative amplitude f_c decreases when the slow mode appears, as shown in Figure 6.

The slow mode slows down critically according to the Ising model as we approach the critical temperature. The fast mode in the high temperature range is identical to the mode observed previously in ternary systems far from the critical temperature.[9] The first cumulant $\Gamma_I(q)$ of these modes is calculated according to eq 25. The resulting q-dependent diffusion coefficient $D_I(q) = \Gamma_I(q)/q^2$ is plotted as a function of q in Figure 7a. In the high q region the plots are linear, suggesting that $\Gamma_I(q) \sim q^3$. This q behavior appears clearly in Figure 7b where $\Gamma_I(q)/q^3$ is represented as a function of q.

4.3. Combined Static and Dynamic Properties. In the high q range the frequencies scale at all measured temperatures with the cube of the scattering wavevector q. From the $\Gamma_I(q) \sim q^3$ region marked in Figure 7b we can determine the viscosity of the solution at higher temperatures. For the lowest two temperatures all the data points in Figure 7b were used. This is done by writing the asymptotic limit in the q^3 region, namely $\Gamma_I(q)/q^3 = kT/(6\pi\eta)$, which gives a direct access to the viscosity of the solution at each temperature. We find a drastic increase of η when T approaches T_c. A preliminary investigation of this behavior shows that the viscosity tends to diverge according to the power law $\eta \sim \epsilon^{-\kappa}$ where the exponent $\kappa \cong 0.29$, as shown in Figure 8. To our knowledge such a scaling law has not been reported elsewhere in the case of a ternary mixture of a polymer blend in the presence of a solvent. Pursuing the analysis of the static and dynamic data and combining the measured $D_I(q)$, $S_{xx}(q)$, and η, one can determine the normalized mobility denoted $\mu(q)\eta$ and compare the results with the predictions of the mode-coupling term in eqs 12 and 13 (neglecting the Rouse contribution given by the quantity $\Phi/3\pi a$).

$$\mu(q)\eta = \frac{1}{4\pi^2}\int_0^\infty dq'\, f\left(\frac{q'}{q}\right) S_{xx}(q') \qquad (28)$$

Figure 9 shows the measured normalized mobility as a function of q, and the symbols for different temperatures are the same as those used in the previous figures. The solid line represents the theoretical prediction given by eq 28. The integration of this equation is performed numerically using the measured structure factors $S_{xx}(q)$ at different temperatures. We recall that the correlation functions measured in the immediate vicinity of T_C exhibit a bimodal distribution. However, the main contribution is due to the slow mode, especially at low q's, as can be seen from Figures 1b, 4, 5, and 6. In the last figure the relative amplitudes of the modes are given for the three lowest temperatures. The extrapolated value to $q = 0$ of the amplitude of the slow mode is not very different from the integrated intensity. The dynamic correlation length ξ_d obtained according to the usual definition $D_I(q)_{q\to 0} = (\Gamma_I/q^2)_{q\to 0} = kT/6\pi\eta\xi_d$ is comparable to the static correlation length ξ at all temperatures. However, the q^2 region at low temperatures is not sufficiently broad (Figure 7a) to allow for an accurate determination of ξ_d and its scaling behavior with ϵ.

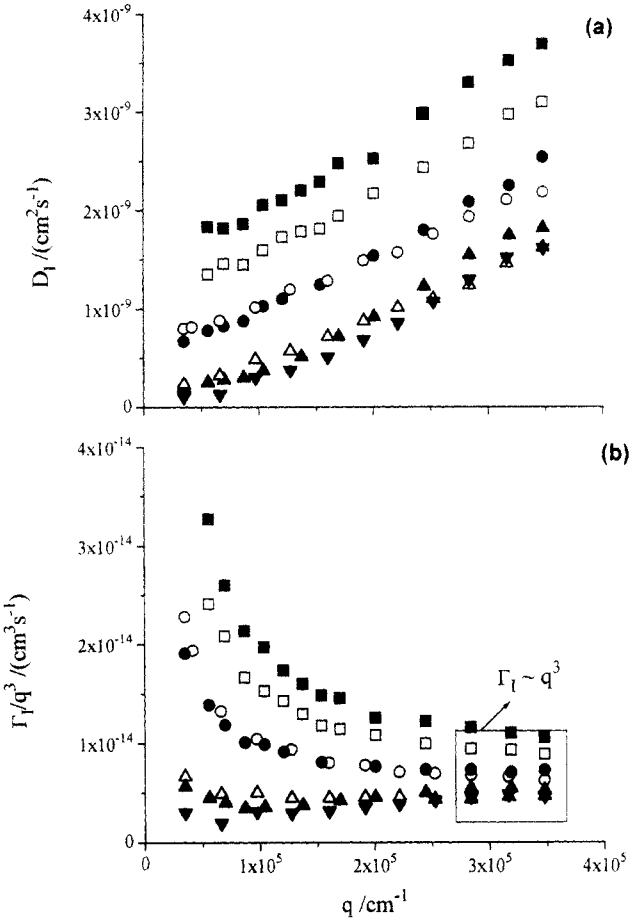

Figure 7. (a) Interdiffusion coefficient as a function of q for different temperatures. It is calculated from a weighted average of the two dominant modes. The symbols mark the following temperatures: (■) 30 °C, (□) 20 °C, (●) 10 °C, (○) 7 °C, (▲) 5 °C, (△) 4 °C, and (▼) 3 °C. (b) Corresponding plot of Γ_I/q^3 versus q. The meaning of the symbols is the same as in Figure 7a. At scattering vector lengths from 2.75×10^5 to 3.5×10^5 cm^{-1} Γ_I is proportional to q^3 for all temperatures measured. The region designated by the square was used to determine the viscosity of the mixture.

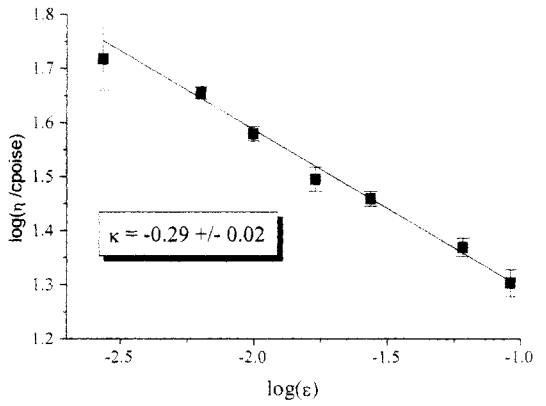

Figure 8. Power law behavior of the solution viscosity as obtained from the q^3 region of Figure 7b. The exponent is indicated in the figure.

5. Discussion and Conclusions

The results obtained from both static and dynamic light scattering measurements show that there are two distinct ranges of temperature where the system has a different behavior. In the upper range from 7 to 30 °C the mean-field picture gives a correct description of the data. This observation is consistent with the work reported earlier[8-11] describing the static and dynamic properties of ternary

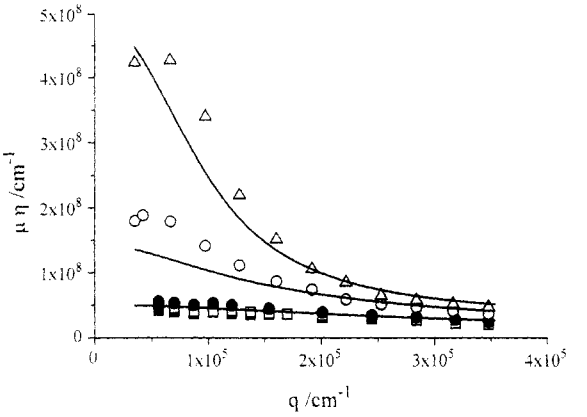

Figure 9. Variation of the mode-coupling part of the mobility μ times the viscosity η as a function of q for different temperatures. The mobility is calculated from the experimental $D_I(q)$ and $S_{xx}(q)$. The viscosity is obtained from Figure 8. The symbols △, ○, ●, □, and ■ represent experimental values at temperatures of 4, 7, 10, 20, and 30 °C, respectively. The solid lines from top to bottom represent the curves calculated from eq 28. They are calculated for temperatures of 4, 7, and 20 °C respectively. The integration is performed numerically using the experimental structure factor S_{xx}.

mixtures at room temperature and in terms of other important parameters such as the mean concentration and composition of the blend. In the lower temperature range close to the critical point (below 7 °C in our case), the mean-field approximation breaks down, as is evident from the critical exponents for the forward scattering intensity and the correlation length, which are close to their Ising values. However the failure of the mean-field picture based on the RPA is expected near T_C since the effects of fluctuations are neglected.

The dynamic correlation function shows a bimodal distribution in the lower temperature range. The fast mode appears at all temperatures and does not seem to show any critical slowing down. The slow mode which appears at 7 °C and below shows the properties of the critical slowing down. Such a behavior is clearly established from the measured correlation functions. In the high temperature range slow and fast modes merge together and the amplitude of the resulting single peak depends on the mean composition, as has been shown by Giebel et al.[9] None of the additional very low amplitude peaks in the frequency distribution increases in amplitude or changes position. These secondary peaks may be due to the total concentration fluctuations because the optical Θ and the symmetry conditions are not strictly fulfilled.

The proper treatment of the static light scattering data requires the correction for the noncritical background, which can be estimated only from the dynamic data.

At low temperatures, a change of slope in the Ornstein–Zernike plot (Figure 1b) is observed. This may be attributed to a variation of the radius of gyration with the temperature, which was not taken into account here. It has been shown theoretically that close to the critical point the mean force acting on a polymer chain becomes very strong and results in shrinking or eventually collapse of the chain.[20] Such a behavior has been experimentally observed on minority chains in the network of majority chains by Monte Carlo simulations.[21] This chain collapse may have an effect on the scaling behavior of the correlation length.

After this paper was submitted, a static light scattering study was reported on a similar system by Miyashita et al.[22]

Acknowledgment. M.B. thanks E.W.F. for his kind invitation to the Max-Planck-Institut für Polymerforschung and for making this collaboration possible.

References and Notes

(1) Wheeler, L. M.; Lodge, T. P. *Macromolecules* **1989**, *22*, 3399. Hanley, B.; Tirell, M.; Lodge, T. P. *Polym. Bull.* **1985**, *14*, 137. Sillescu, H. *Makromol. Chem., Rapid Commun.* **1984**, *5*, 519. Martin, J. E. *Macromolecules* **1984**, *17*, 1279. Akcasu, Z. A.; Hammouda, B.; Lodge, T. P.; Han, C. C. *Macromolecules* **1984**, *17*, 759.
(2) Benmouna, M.; Benoit, H.; Duval, M.; Akcasu, Z. A. *Macromolecules* **1987**, *20*, 1107.
(3) Benmouna, M.; Seils, J.; Meier, G.; Patkowski, A.; Fischer, E. W. *Macromolecules* **1993**, *26*, 668.
(4) Roby, F.; Joanny, J. F. *Macromolecules* **1992**, *25*, 4612.
(5) Stepanek, P.; Lodge, T. P.; Kedrowski, C.; Bates, F. S. *J. Chem. Phys.* **1991**, *94*, 8289. Bates, F. S.; Rosedale, J. H.; Stepanek, P.; Lodge, T. P.; Wiltzius, G. H.; Frederickson, G. H.; Hjelm, R. P., Jr. *Phys. Rev. Lett.* **1990**, *65*, 1893.
(6) Meier, G.; Momper, B.; Fischer, E. W. *J. Chem. Phys.* **1992**, *97*, 5884.
(7) Janssen, S.; Schwahn, D.; Springer, T. *Phys. Rev. Lett.* **1992**, *68*, 3180.
(8) Borsali, R.; Duval, M.; Benmouna, M. *Macromolecules* **1989**, *22*, 816.
(9) Giebel, L.; Borsali, R.; Fischer, E. W.; Meier, G. *Macromolecules* **1990**, *23*, 4054. Giebel, L.; Borsali, R.; Fischer, E. W.; Benmouna, M. *Macromolecules* **1992**, *25*, 4378. Giebel, L.; Benmouna, M.; Borsali, R.; Fischer, E. W. *Macromolecules* **1993**, *26*, 2433. Konák, C.; Tutar, Z.; Jakes, J. *Polym.* **1990**, *31*, 1866. Brown, W.; Zhou, P. *Macromolecules* **1990**, *23*, 5097.
(10) Daivis, P. J.; Pinder, D. N. *Macromolecules* **1993**, *26*, 3381.
(11) Aven, M. R.; Cohen, C. *Macromolecules* **1990**, *23*, 476.
(12) de Gennes. *Scaling Concepts in Polymer Physics*; Cornell University Press: Ithaca, NY, 1979.
(13) Akcasu, Z. A. In *Dynamic Light Scattering: The Method and Some Applications*, Brown, W., Ed.; Pergamon: Oxford, U.K., 1992. Akcasu, Z. A.; Nägele, G.; Klein, R. *Macromolecules* **1991**, *24*, 4408.
(14) Doi, M.; Edwards, S. F. *Theory of Polymer Dynamics*; Clarendon Press: Oxford, U.K., 1986.
(15) Mori, H. *Prog. Theor. Phys.* **1965**, *34*, 399. Zwanzig, R. *J. Chem. Phys.* **1974**, *60*, 2717.
(16) Momper, B. Ph.D. Thesis, The University of Mainz, 1989.
(17) Bender, T. M.; Lewis, R. J.; Pecora, R. *Macromolecules* **1986**, *19*, 244.
(18) Shanks, J. G.; Sengers, J. V. *Phys. Rev. A* **1988**, *38*, 885.
(19) Provencher, S. W. *Comput. Phys. Commun.* **1982**, *27*, 213, 229.
(20) Brereton, M. G.; Vilgis, T. A. *J. Phys. (France)* **1989**, *50*, 245.
(21) Sariban, A.; Binder, K. *Makromol. Chem.* **1988**, *189*, 2357.
(22) Miyashita, N.; Okada, M.; Nose, T. *Polymer* **1994**, *35*, 1038.